Heterogeneous twinning during directional solidification of multi-crystalline silicon

J. W. Jhang, Gabrielle Regula, Guillaume Reinhart, Nathalie Mangelinck-Noël, C. W. Lan

Heterogeneous Twinning during directional solidification of multi-crystalline silicon

J.W. Jhang[a], G. Regula[b], G. Reinhart[b], N. Mangelinck-Noël[b], C.W. Lan[a]*

[a]Department of Chemical Engineering, National Taiwan University, Taipei, 10617, Taiwan

[b] Aix Marseille Univ, Université de Toulon, CNRS, IM2NP, Marseille, France

*Corresponding author: cwlan@ntu.edu.tw; Tel.: 886-2-2363-3917

Fax: 886-2-2363-3917

Abstract

Heterogeneous twinning nucleation from the wall or gas interface during directional solidification of silicon have been modelled, and further used to clarify the details of twining observed *in situ* in X-ray synchrotron imaging experiments [1]. It is found that the heterogeneous twinning from the wall/grains or wall/gas/grain trijunctions requires much lower undercoolings leading to much higher twinning probability. The lower attachment energy and the contact area are the key factors for the heterogeneous nucleation of twins.

Keywords: A1. Twinning; A1. Heterogeneous; A1. Undercooling; A1. Facets; A1. Nucleation

1. Introduction

Twin boundaries in silicon have attracted much attention in recent years due to their significance in solar cells [1-3]. Most of the twin boundaries in silicon are issued from Σ3 twin nucleation on {111} facets [4, 5], which has been studied extensively [6-9]. Among them, the *in situ* observations through synchrotron X-ray [1-2] have revealed dynamic features of the twin formation from facets, as well as the defect formation related to the twinning, during directional solidification of silicon slabs in a boron nitride crucible. Nevertheless, the role of the crucible wall and of the gas phase has not yet been understood during twinning. To understand the detailed nucleation mechanisms, heterogeneous twin nucleation models are necessary.

Duffar and Nadri [10] were the first to extend the Voronkov model [11] to study twinning during the growth of multi-crystalline silicon (mc-Si). Recently, Lin and Lan [12] revised this model by considering the interaction between the nucleus and the neighboring grain. With this modification, referred as Lin's model, an estimated undercooling of around 1 K for noticeable twining could be obtained which is consistent with the literature reported values although slightly higher [13]. Nevertheless, this model showed that the interaction of the nucleus with the neighboring grains was significant, and the grain boundary (GB) with the twinned grain on the {111} growth facets was a crucial factor. In addition, Lin and Lan [12] mentioned that most twin crystals nucleated from the facet-facet groove at the trijunction (TJ), especially from the non-∑ GBs due to the larger undercooling in the deeper groove. This model explained the nucleation and twinning mechanism at the solid-solid-liquid TJ (SSL-TJ) but was first applied to a 2D configuration. To further

explain the more realistic situation of the three-grain tri-junctions (3GTJ) on the interface during ingot growth, Jain et al. [14], further developed a three-dimensional model, referred as Jain's model. With the 3GTJ model, the twinning from certain grains during mc-Si growth experiments [15] was correctly predicted. More importantly, the required undercooling for twining was in the order of 0.3 K, which was consistent with the measured value [2, 13].

In this paper, we extend Jain's model [14] to the heterogeneous twinning. The cases involving the wall/grains, wall/gas/grain, and gas/grain junctions are modeled and discussed. The models are further used to explain the possible twinning locations characterized during *in situ* X-ray synchrotron imaging experiments [1, 2]. The detailed model developed is described in the next section. Section 3 is developed to results and discussion, followed by conclusions in Section 4.

2. Heterogeneous twinning model

In general, there are several possible heterogeneous twinning situations during directional solidification observed as well in experiments [1, 2], as summarized in Fig. 1(a), where the schematic of the slab growth is shown on the left figure. As shown, model 1-1 considers two facets in contact with the crucible wall, so that there is a wall/G1/G2 TJ and a GB exists between G1 and G2. This model is similar to Jain's model by replacing the third grain by the crucible wall. In model 1-2, there is only one facet in contact with the wall, which occurs on the edge facet. Model 2 takes the gas phase into consideration. Again, there are two cases for twin nucleation as shown in the figure: one involves the wall/grain/gas TJ (model 2-1), and the other simply

considers the nucleation from the facet/gas contact line (model 2-2). The force balances at the junctions for different models are described schematically in Fig. 1(b).

We first consider two facets in contact with the wall (model 1-1), as shown in Fig. 2. The schematic of the facet and GB planes are shown in Fig. 2(a) and of a nucleus viewed from the top in contact with the facet, as well as the force balances at the junctions, are depicted in Fig. 2(b). Again, the nucleus is assumed to be a circular disc on the facet, as in Jain's model [14]. Therefore, the angles defined are based on the view angle normal to the facet, or the angles are normal to the facet. As shown in Fig. 2(a), each grain contributes with a {111} facet at the TJ, and the facets may not have the same size. The GB plane is assumed to be parallel to the direction of solidification, which is generally true for random angle GBs after grain competition during growth [10]. In addition, the angle θ could be calculated from the normal vectors of the GB plane and the crucible wall. Again, for the convenience of the discussion, we assume that the GB is normal to the wall, i.e., $\theta = 90^{o}$, without losing the generality. In Hurle's model [16], the first criterion for a facet growth nucleus to attach at the TJ is that the free energy γ_e associated with a step attaching the TJ needs to be lower than the normal step free energy γ_{step}. Because in the model 1-1, there are two steps from G1 and G2, the criterion for two steps anchoring at the TJ becomes $\gamma_e^{12} < 2\gamma_{step}$, which is similar to Lin's and Jain's models. The interaction between a nucleus step coming from G1 or G2 and the surface of the wall, i.e., the facet-wall groove, also needs to be considered. Hence, $\gamma_e^{12}, \gamma_e^{1w}$ and γ_e^{2w} could be calculated as follows:

$$\gamma_e^{12}h = [\sigma_{GB} - \sigma_{SL}^{111}\cos(180° - \nu_1) - \sigma_{SL}^{111}\cos(180° - \beta_1)]\frac{h}{\sin(180°-\nu_1)}, \quad (1)$$

$$\gamma_e^{1w}h = [\sigma_{WS} - \sigma_{SL}^{111}\cos(180° - \nu_2) - \sigma_{WL}]\frac{h}{\sin(180°-\nu_2)}, \quad (2)$$

$$\gamma_e^{2w}h = [\sigma_{WS} - \sigma_{SL}^{111}\cos(180° - \beta_2) - \sigma_{WL}]\frac{h}{\sin(180°-\beta_2)}, \quad (3)$$

where σ_{GB} is the GB energy. The superscript 1w or 2w indicates the junction between G1 or G2 and the crucible wall. For silicon, σ_{GB} is in the range of 0.45~0.5 J/m^2 at 1473 K as reported in the experiments by Otsuki [17]; here we again pick 0.4842 J/m^2, which was a fitting parameter used previously [14]. Also, σ_{SL}^{111} is the surface free energy of a {111} plane, and according to Hurle [16] the value is 0.257 J/m^2. In addition, h (0.324 nm) is the height of an atomic silicon layer in the [111] direction. Moreover, σ_{WS} (0.473 J/m^2) and σ_{WL} (0.372 J/m^2) are the surface energies at the wall/solid and wall/melt interfaces, respectively. The facet angles ν_1 and β_1 are the angle between the facets and the GB plane as shown in Fig. 2(a); ν_2 and β_2 are the angle between the facets and the wall; the angle β_1 is usually not equal to ν_1 unless the GB plate is perpendicular to the wall. Once the growth direction is known, e.g., in $< 100 >$ direction, in the reference coordinate, the facet angles can be easily calculated. The grain orientations could be obtained from the Electron Backscatter Diffraction (EBSD) data.

The next step is to calculate the free energy to create the critical nucleus. The angle ϕ_{GB}, ϕ_1, and ϕ_2 in Fig. 2(b) can be determined by the force balances at the junctions as shown on the right of the figure. The required volume and the surface

area for the nucleus on the facet as shown in Fig. 2(c) can be calculated as explained in [14]. In Fig. 2(c), the angles, normal to the facet, with the superscript prime indicate they are defined at the top surface of the nuclei. Then, the free energy of formation for the facet nucleus can be calculated as follows:

$$\Delta G_F = (\Delta S \Delta T)\Sigma V^i + \gamma_{step} \cdot \Sigma A^i_{step} + \Sigma \gamma_e^{iw} \cdot A^{iw}_{edge} + \gamma_e^{12} \cdot A^{12}_{edge}\,, \tag{4}$$

where

$$\Sigma A^i_{step} = A^1_{step} + A^2_{step} \tag{5}$$

and

$$\Sigma \gamma_e^{iw} \cdot A^{iw}_{edge} = \gamma_e^{1w} \cdot A^{1w}_{edge} + \gamma_e^{2w} \cdot A^{2w}_{edge}\,. \tag{6}$$

In Eq. (4), ΔS is the entropy of solidification ($-2.68 \cdot 10^6$ J m^{-3} K^{-1}) and ΔT is the undercooling. ΣA^i_{step} and ΣV^i are the area of the surface steps and volume of the truncated nucleus, respectively; A^{iw}_{edge} is the area of the edge of the truncated nucleus between the crucible wall and the nucleus i ($i = 1$ and 2), and A^{12}_{edge} is the area of the edge of the truncated nucleus between G1 and G2.

Figure 3(a) shows the plot of the Gibbs free energy required for the facet nucleation for an undercooling of 2.8 K with the facet angle $\nu_1 = 150°$; $\beta_1 = \nu_1$, and $\nu_2 = 110°$; $\beta_2 = \nu_2$. The comparison is also made with Jain's model [14]. As shown, the radius of the critical nucleus and the energy barrier in model 1-1 are much smaller than that in Jain's model. The main reason is that the additional contact energy with the wall ($\sigma_{WS} - \sigma_{WL}$) is much smaller than σ_{GB}, which eases nucleation. As a consequence, the attaching energy in model 1-1 is lower.

Furthermore, if the nucleus from G1 is twinned, the twin energy needs to be

taken into account, while the facet on G2 keeps the same orientation. Then, the free energy of formation for a twinned nucleus can be written as:

$$\Delta G_T = (\Delta S \Delta T)\Sigma V^i + \gamma_{step} \cdot \Sigma A^i_{step} + \Sigma \gamma_e^{iw} \cdot A^{iw}_{edge} + \gamma_e^{12} \cdot A^{12}_{edge} + \sigma_{twin} \cdot A^1_{bottom}, \quad (7)$$

where σ_{twin} is the energy for forming a twin plane at the bottom of the nucleus on G1 and A^1_{bottom} is the bottom contact area of the twin grain nucleus with the parent grain. Other terms in Eq. (7) are the same as those in Eq. (4). For comparison purposes, we utilize the twinning energy of 2 mJ/m^2 as used in [14]. It should be mentioned that the twin energy was predicted to be around 20 to 60 mJ/m^2 at 0 K for silicon [18]. However, the value is most likely much smaller near the melting temperature (1683 K) as the examples discussed in [14]. Moreover, the Gibbs free energy for twin nucleation is plotted in Fig. 3(b). As shown, both the Gibbs free energy and the critical radius for twin nucleation are higher than that for facet growth studied above. As compared with Jain's model, the twin nucleation is easier because of the additional contribution from the wall. After the free energy barriers of formation for the faceted and twinned nuclei are obtained, we can further calculate the twinning probability according to [10] as:

$$P_T = \frac{e^{\frac{-\Delta G^*_T}{kT}}}{e^{\frac{-\Delta G^*_F}{kT}} + e^{\frac{-\Delta G^*_T}{kT}}}, \quad (8)$$

where ΔG^*_F and ΔG^*_T are the free energy barriers for facet and twin nucleation, respectively; k is the Boltzmann constant. The twinning probability as a function of the undercooling is shown in Fig. 3(c), where the probability based on Jain's model is put together for comparison. As shown, the probability of twinning in model 1-1 is

higher than that in Jain's model for all undercooling.

The effect of the facet angles (ν_1 and ν_2) on the twinning probability has been further studied and data are gathered in Fig. 4. As shown, with a larger facet angle, for a given twinning probability, the required undercooling is smaller. Again, this is due to the effect of the angle on the truncated volume and of the smaller A^1_{bottom}. As shown in Fig. 4, with $\nu_1 = 165°$ and $\nu_2 = 110°$, the critical undercooling for frequent twin nucleation ($P_T \sim 10^{-5}$) is around $0.4 - 0.5$ K in model 1-1, and this undercooling is consistent with the value estimated from the experiments ($0.3 - 0.6$ K) [13].

Model 1-2 is a simplified case of model 1-1, which is shown in Fig. 1(a) for the facet at the edge. Because there is only one facet in contact with the wall, the free energy γ_e^{1w} associated with a step attaching the junction, the free energies of formation for the faceted and twinned nucleus can be calculated as follows:

$$\gamma_e^{1w} h = [\sigma_{WS} - \sigma_{SL}^{111}\cos(180° - \nu_2) - \sigma_{WL}]\frac{h}{\sin(180°-\nu_2)}, \quad (9)$$

$$\Delta G_F = (\Delta S \Delta T)V + \gamma_{step} \cdot A^1_{step} + \gamma_e^{1w} \cdot A^{1w}_{edge}, \quad (10)$$

$$\Delta G_T = (\Delta S \Delta T)V + \gamma_{step} \cdot A^1_{step} + \gamma_e^{1w} \cdot A^{1w}_{edge} + \sigma_{\text{twin}} \cdot A^1_{bottom}. \quad (11)$$

Similarly, the twinning probability for different undercoolings could also be calculated. For the same angle, e.g. ν_2=110^o, the required undercooling for twining is about 5 to 6 K for model 1-2 having a probability of 10^{-5} as compared to 2 K in model 1-1. Similarly for the same undercooling , the twinning probability increases as the facet angle increases. Again, this is due to the smaller attaching energy γ_e^{1w} and to the contact area.

Next we consider the wall/grain/gas trijunction (model 2-1) as presented in Fig. 1 for the facet at the edge. Similarly, the criterion for the occurrence of facets at the junction is that the free energies γ_e^{1w} and γ_e^{1g} associated with a step attaching the junction needs to be lower than the normal step free energy. Thus, the attaching energies γ_e^{1w}, γ_e^{1g}, and the free energies of formation for the faceted and twinned nuclei can be written as:

$$\gamma_e^{1w} h = [\sigma_{WS} - \sigma_{SL}^{111}\cos(180° - \nu_2) - \sigma_{WL}]\frac{h}{\sin(180°-\nu_2)}, \tag{12}$$

$$\gamma_e^{1g} h = \left[\sigma_{gS} - \sigma_{SL}^{111}\cos(180° - \nu_3) - \sigma_{gL}\right]\frac{h}{\sin(180°-\nu_3)}, \tag{13}$$

$$\Delta G_F = (\Delta S \Delta T)V + \gamma_{step} \cdot A_{step}^1 + \gamma_e^{1w} \cdot A_{edge}^{1w} + \gamma_e^{g} \cdot A_{edge}^{1g}, \tag{14}$$

and

$$\Delta G_T = (\Delta S \Delta T)V + \gamma_{step} \cdot A_{step}^1 + \gamma_e^{1w} \cdot A_{edge}^{1w} + \gamma_e^{1g} \cdot A_{edge}^{1g} + \sigma_{twin} \cdot A_{bottom}^1, \tag{15}$$

where the facet angle ν_3 is the angle between the facet and the gas, and σ_{gS} (0.604 J/m^2) and σ_{gL} (0.75 J/m^2) are the gas/crystal and gas/melt interfacial energies, respectively； A_{edge}^{1w} and A_{edge}^{1g} are the edge areas of the truncated nucleus on the wall and gas sides, respectively. For ν_2 =110^o, ν_3 =60^o, and θ =50^o, the required undercooling for twining is about 3.2 K for model 2-1 having a probability of 10^{-5} as compared to 2 K in model 1-1; the contact angle θ is the angle between the crystal edge and the wall. Similar to the previous cases, the twinning probability increases with the increasing facet angles due to the lower attaching energy and to the lower contact area. The contact angle θ induces a similar trend. As the contact angle θ

decreases, the twinning probability increases as a result of the lower contact area.

Model 2-2 is a simplified case of model 2-1, which considers the nucleation from the facet/gas contact line as shown in Fig. 1. The free energy γ_e^{1g} associated with a step attaching the junction, the free energy of formation for the faceted and twinned nucleus can be formulated as follows:

$$\gamma_e^{1g} h = \left[\sigma_{gS} - \sigma_{SL}^{111}\cos(180° - \nu_3) - \sigma_{gL}\right]\frac{h}{\sin(180°-\nu_3)}, \quad (16)$$

$$\Delta G_F = (\Delta S \Delta T)V + \gamma_{step} \cdot A_{step}^1 + \gamma_e^{1g} \cdot A_{edge}^{1g}, \quad (17)$$

and

$$\Delta G_T = (\Delta S \Delta T)V + \gamma_{step} \cdot A_{step}^1 + \gamma_e^{1g} \cdot A_{edge}^{1g} + \sigma_{twin} \cdot A_{bottom}^1. \quad (18)$$

The twinning probability curves with the effect of the facet angle as a function of the undercooling are similar to model 2.1, but the undercooling is about 1.5 K higher for the similar angles, i.e., $\nu_3 = 60^o$. Again, the higher facet angle ν_3 leads to the higher twinning probability due to the smaller attaching energy γ_e^{1g} and lower contact area.

3. Results and discussion

To validate our models, three cases from the experiments developed by the IM2NP team [1, 2, 19] are selected for comparison. We first consider one experiment of growth from a seed oriented <100> in the solidification direction and presented in details in [2, 19]. The EBSD map of the final grain structure is shown in Fig. 5(a). For this experiment, two cases labeled as Cases 1 and 2 are considered. The Case 1 corresponds to nucleation in a grain boundary groove, i.e. similar to model 1-1. As

shown by the *in situ* X-ray imaging during this experiments, the Σ3 twin grain (purple on the inverse pole figure EBSD map Fig. 5) nucleates on the {111} facet of G1 in the grain boundary groove, instead of the one of G2. The enlarged figure of Case 1 is shown in Fig. 5(b), while Case 2 in Fig. 5(c). The evolution of a typical facetted/facetted groove at the solid-liquid interface during directional solidification in the same experiment was described by Stamelou et al. [2]. With a sufficient undercooling, a twin grain can nucleate on one of the facets. However, there are two possibilities for this twinning: at the G1/G2 GB away from the wall or at the G1/G2/wall TJ. For the former case, Lin's 2D model [12] is a proper one to apply because the bisector rule could be adopted for Case 1. However, for the latter, we need to apply model 1-1. To predict the correct site for twin nucleation, we need to compare the twinning probability of both models under the same undercooling.

The corresponding Euler angles of G1 (parent grain), G2 and twin grain obtained from EBSD are listed in Table 1(a). The eight [111] vectors of each grain could be obtained from its Euler angles, and so as the corresponding facet angles ν_1, β_1, ν_2 and β_2 shown in Fig. 2(a). Again, we assume the GB angle θ to be 90° in the calculation, and the GB energy (σ_{GB}) is chosen to be 0.48 J/m^2 [12]. With the facet angles and σ_{GB}, the attaching energies could be calculated as described previously. The corresponding facet angles and the attaching energy values associated with facet 1 and facet 2 of model 1-1 and 2D nucleation model are listed in Table 1(b) and (c), respectively. It can be seen that for both facets of model 1-1, the attaching energy to the nucleus/grains/wall TJ is negative and that for facet 1, it is slightly lower due to the larger facet angle in contact with the wall. The free energies of formation for a

twinned nucleus for both facets for model 1-1 are significantly lower than Lin's 2D model with the observed undercooling (ΔT = 0.35 K), and the critical radius of the twin nucleus is about 2.1 nm.

The energy barrier for the twining on facet 1 of model 1-1 turns out to be the lowest; the barrier for facet 2 should be the same if the bisector rule is applied. Accordingly, the twinning probability (8×10^{-7}) is the highest in the three situations. The contact area and probability of twinning calculated by both models for Case 1 are listed in Table 1(d). As shown, beside the probability, the corresponding contact area of the nucleus on facet 1 is also the lowest one. Because the twin energy term is the lowest, the twinning is more likely to occur at facet1/GB/wall TJ. On the contrary, with the undercooling of 0.35 K, we could not find an energy barrier of twinning on the facet based on Lin's 2D model within a reasonable nucleus size, so that the twinning is not likely. Therefore, we could conclude that for Case 1 the twinning on facet 1 at the G1/GB/wall TJ is the most thermodynamically favorable at the measured undercooling, and this is consistent with the experimental result.

For Case 2 in Fig. 5(c), the twin formation from both $\{111\}$ facets appear at the edges of the solid-liquid interface. For this case, we focus on the twinning phenomenon on the left hand side of the graph and test model 2-1 (facet/gas/wall TJ) or model 2-2 (facet/gas contact line) for predicting the twinning probability. The corresponding Euler angles of the parent (G1) and twin grains are also obtained from EBSD data, as listed in Table 2(a). The corresponding facet angles could then be calculated as presented in Table 2(b). We set the angle θ to be $45°$ for model 2-1 for the calculation. Following the previously mentioned procedure for model 2-1 and 2-2,

the attaching energy values, contact area and twinning probabilities associated with the {111} facet are calculated and listed in Table 2(c) and (d). It can be seen that the facet of model 2-1 has a positive γ_e^{1w} value, which would increase the energy barrier of formation for a twinned nucleus, but the bottom contact area of the nucleus in model 2-1 is much lower than that in model 2-2. In addition, the contribution of the twin energy is also lower to the energy barrier of twinning on the facet in model 2-1. As a result, the energy barrier for twinning from model 2-1 is slightly lower, but the difference is quite small. The critical radius for twinning is 22 nm for model 2-1 and 23 nm for model 2-2 at an undercooling of 4 K. Thus, the twinning at the facet/gas/wall TJ is more likely than that at the facet/gas contact line. The undercooling in the model needs to be higher (4 K). In the experiments [2], the undercooling at the edge is indeed higher than in the grain boundary grooves and this is revealed by the larger facets observed. However, the measured values were always lower than 1 K which implied that twin nucleation occurred before an undercooling of 4 K was reached. It could also mean that an additional mechanism eases nucleation as the presence of defects on the {111} facet such as dislocations and/or the presence of impurities.

The last case is shown in Fig. 6, where the EBSD map in Fig. 6(a) is from [1] and the area inside the box is labeled as Case 3 in the following. The schematic of the twin formation during crystal growth is illustrated in Fig. 6(b), where the twin grain appears form the left and continues to grow to the right. For this case, the twin could nucleate from facet/wall contact line (model 1-2) or from facet/gas/wall TJ (model 2-1). The corresponding Euler angles of the parent grain (G1) and of the twin grain are

also obtained by EBSD and summarized in Table 3(a) and the calculated facet angles for both models are listed in Table 3(b); the angle θ in model 2-1 is assumed to be 45° in the calculation.

The attaching energy values, contact area and twinning probability associated with the facet in both models are listed in Table 3(c) and (d). It can be seen that model 2-1 has a negative attaching energy, which would help to decrease the energy barrier for twinning. In addition, the bottom contact area of the nuclei in model 2-1 is lower than that in model 1-2, so that the contribution of twin energy is also lower to the nucleation barrier in model 2-1. The energy barrier for the twin nucleation from the facet/gas/wall TJ (model 2-1) is indeed lower than that from the facet/gas junction (model 2-2); the undercooling is set at 2.6 K. The critical radius for twining is 47 nm at the facet/gas/wall TJ, which is only half of that at the facet/gas contact line. The twinning probability in Table 3(d) further indicates that the twinning from the facet/gas/wall TJ is more favorable as also demonstrated for the same situation in Fig. 5.

4. Conclusions

In this study, the 3GTJ model proposed by Jain et al. [14] is extended to the heterogeneous twinning considering the wall and gas boundaries; the models are developed for the wall/grains/GB, wall/grain, wall/gas/grain, and gas/grain TJs. It is observed that the radius of critical truncated nucleus and the energy barrier in model 1-1 (wall/G1/G2 TJ) are much smaller than that in Jain's 3GTJ model. The models are further utilized to predict the possible twinning sites in experiments [1, 2], and show

good agreement including the predicted undercooling. It is found that twin grain nucleation probability is higher at the edge of the sample and/or at the crucible walls, where the attaching energy and the bottom contact area of the twin nucleus tend to be lower which is as well in nice agreement with what is generally observed during directional solidification.

Acknowledgement

This work was supported by the Ministry of Science and Technology of Taiwan for the group in Taiwan and by the French National Research Agency (ANR) with Project CrySaLID (No ANR-14-CE05-0046-01). The collaboration between both groups was sustained in both countries by the PhD ORCHID framework (project No 35898SB).

References

[1] M.G. Tsoutsouva, T. Riberi-Beridot, G. Regula, G. Reinhart, J. Baruchel, F. Guittonneau, L. Barrallier, N. Mangelinck-Noel, *In situ* investigation of the structural defect generation and evolution during the directional solidification of < 110 > seeded growth Si, Acta Mater. 115 (2016) 210-223.

[2] V. Stamelou, M.G. Tsoutsouva, T. Riberi-Beridot, G. Reinhart, G. Regula, J. Baruchel, N. Mangelinck-Noel, {111} facet growth laws and grain competition during silicon crystallization, J. Cryst. Growth 479 (2017) 1-8.

[3] H.J. Moller, C. Funke, M. Rinio, S. Scholz, Multicrystalline silicon for solar cells, Thin Solid Films 487(1-2) (2005) 179-187.

[4] K. Nagashio, K. Kuribayashi, Growth mechanism of twin-related and twin-free facet Si dendrites, Acta Mater. 53(10) (2005) 3021-3029.

[5] C.I. Drowley, G.A. Reid, R. Hull, Model for facet and sidewall defect formation during selective epitaxial-growth of (001) silicon, Appl. Phys. Lett. 52(7) (1988) 546-548.

[6] L.Csepregi, E.F. Kennedy, J.W. Mayer, Substrate-orientation dependence of the

epitaxial regrowth rate from Si-implanted amorphous Si, Appl. Phys. Lett. 49(7) (1978) 3906-3911.
[7] C.W.T. Bulle-Lieuwma, A.H. van Ommen, L.J. van IJzendoorn, Microstructure of heteroepitaxial Si/$CoSi_2$/Si formed by Co implantation into (100) and (111) Si, Appl. Phys. Lett. 54(3) (1989) 244-246.
[8] A. Bourret, J.J. Bacmann, Atomic-structure of grain-boundaries in semiconductors Studied by electron-microscopy (analogy and differences with surfaces), Surf. Sci. 162(1-3) (1985) 495-509.
[9] A. Garg, W.A.T. Clark, J.P. Hirth, Dissociated and faceted large-angle coincident-site-lattice boundaries in silicon, Philos.. Mag A 59(3) (1989) 479-499.
[10] T. Duffar, A. Nadri, On the twinning occurrence in bulk semiconductor crystal growth, Scripta. Mater. 62(12) (2010) 955-960.
[11] V. V. Voronkov, Processes at the boundary of a crystallization front, Sov. Phys . Crystallogr. 19 (1975) 573-577.
[12] H.K. Lin, C.W. Lan, Revisiting the twinning mechanism in directional solidification of multi-crystalline silicon sheet, Acta Mater. 131 (2017) 1-10.
[13] A. Tandjaoui, N. Mangelinck-Noel, G. Reinhart, B. Billia, T. Lafford, J. Baruchel, Investigation of grain boundary grooves at the solid-liquid interface during directional solidification of multi-crystalline silicon: *in situ* characterization by X-ray imaging, J. Cryst. Growth 377 (2013) 203-211.
[14] T. Jain, H.K. Lin, C.W. Lan, Twinning mechanism at three-grain tri-junction during directional solidification of multi-crystalline silicon, Acta Mater. 144(Supplement C) (2018) 41-50.
[15] Y.T. Wong, C. Hsu, C.W. Lan, Development of grain structures of multi-crystalline silicon from randomly orientated seeds in directional solidification, J. Cryst. Growth 387 (2014) 10-15.
[16] D.T.J. Hurle, A Mechanism for Twin Formation during Czochralski and encapsulated vertical bridgman growth of III-V compound semiconductors, J. Cryst. Growth 147(3-4) (1995) 239-250.
[17] A. Otsuki, Energies of (001) twist grain boundaries in silicon, Acta Mater. 49(10) (2001) 1737-1745.
[18] R. Hull, INSPEC, Properties of crystalline silicon, INSPEC, the Institution of Electrical Engineers, 1999.
[19] Thècle Riberi-Béridot, In situ characterization by X-ray synchrotron imaging of the solidification of silicon for the photovoltaic applications: control of the grain structure and interaction with the defects and the impurities, PhD Thesis, Aix Marseille Univ (2017).

Table Captions:

Table 1 (a) The corresponding Euler angles of parent grain (G1), G2 and twin grain; (b) the corresponding facet angles; (c) the attaching energy values associated with both {111} facets for model 1-1 and for 2D nucleation model; (d) the contact area (A_{bottom}) and the probability of twinning calculated by model 1-1 and 2D nucleation model for Case 1.

Table 2 (a) The corresponding Euler angles of parent grain (G1) and twin grain; (b) the corresponding facet angles; (c) the attaching energy values associated with a {111} facet for models 2-1 and 2-2; (d) the contact area (A_{bottom}) and probability of twinning calculated by models 2-1 and 2-2 for Case 2.

Table 3 (a) The corresponding Euler angles of parent grain (G1) and twin grain; (b) the corresponding facet angles; (c) the attaching energy values associated with a {111} facet for models 1-2 and 2-1; (d) the contact area (A_{bottom}) and probability of twinning calculated by models 1-2 and 2-1 for Case 3.

Table 1

Table 1 (a) The corresponding Euler angles of parent grain (G1), G2 and twin grain; (b) the corresponding facet angles; (c) the attaching energy values associated with both {111} facets for model 1-1 and for 2D nucleation model; (d) the contact area (A_{bottom}) and the probability of twinning calculated by model 1-1 and 2D nucleation model for Case 1.

(a)

Euler angles	Parent Grain (G1)	G2	Twin Grain
φ_1	109.20°	69.01°	35.81°
Φ	43.66°	42.75°	42.89°
φ_2	87.41°	89.36°	1.10°

(b)

Model	ν_1	β_1	ν_2	β_2
Model 1-1 Facet 1	160°		131.53°	
Model 1-1 Facet 2		160°		130.51°
2D nucleation model	160°	160°		

(c)

Model	γ_e^{1w}(J/m^2)	γ_e^{2w}(J/m^2)	γ_e^{12}(J/m^2)
Model 1-1 Facet 1	$-9.27 \times 10^{-2} \pm 0.04$		$-8.77 \times 10^{-3} \pm 0.04$
Model 1-1 Facet 2		$-8.66 \times 10^{-2} \pm 0.04$	$-8.77 \times 10^{-3} \pm 0.04$
2D nucleation model			$-8.77 \times 10^{-3} \pm 0.04$

(d)

Model	A_{bottom} (nm^2)	Probability
Model 1-1 Facet 1	681.34	$7.83 \times 10^{-7} \pm 1.5 \times 10^{-30}$
Model 1-1 Facet 2	697.41	$8.27 \times 10^{-8} \pm 1.5 \times 10^{-30}$
2D nucleation model	–	–

Table 2

Table 2 (a) The corresponding Euler angles of parent grain (G1) and twin grain; (b) the corresponding facet angles; (c) the attaching energy values associated with a {111} facet for models 2-1 and s2-2; (d) the contact area (A_{bottom}) and probability of twinning calculated by models 2-1 and 2-2 for Case 2.

(a)

Euler angles	Parent Grain (G1)	Twin Grain
φ_1	356.11°	109.23°
Φ	43.87°	43.67°
φ_2	3.05°	87.41°

(b)

Model	ν_2	ν_3
Model 2-1	92.53°	52.39°
Model 2-2		52.39°

(c)

Model	γ_e^{1w}(J/m^2)	γ_e^{g}(J/m^2)
Model 2-1	$8.97 \times 10^{-2} \pm 0.04$	$1.36 \times 10^{-2} \pm 0.04$
Model 2-2		$1.36 \times 10^{-2} \pm 0.04$

(d)

Model	A_{bottom} (nm^2)	Probability
Model 2-1	824.59	$2.19 \times 10^{-14} \pm 1.5 \times 10^{-30}$
Model 2-2	1937.24	$3.49 \times 10^{-15} \pm 1.5 \times 10^{-30}$

Table 3

Table 3 (a) The corresponding Euler angles of parent grain (G1) and twin grain; (b) the corresponding facet angles; (c) the attaching energy values associated with a {111} facet for models 1-2 and 2-1; (d) the contact area (A_{bottom}) and probability of twinning calculated by models 1-2 and 2-1 for Case 3.

(a)

Euler angles	Parent Grain (G1)	Twin Grain
φ_1	99.84°	343.83°
Φ	0.76°	47.75°
φ_2	36.78°	25.78°

(b)

Model	ν_2	ν_3
Model 1-2	125.69°	
Model 2-1	125.69°	64.32°

(c)

Model	γ_e^{1w}(J/m^2)	γ_e^{g}(J/m^2)
Model 1-2	$-6.02 \times 10^{-2} \pm 0.04$	
Model 2-1	$-6.02 \times 10^{-2} \pm 0.04$	$-3.84 \times 10^{-2} \pm 0.04$

(d)

Model	A_{bottom} (nm^2)	Probability
Model 1-2	4085.54	$7.34 \times 10^{-18} \pm 1.5 \times 10^{-30}$
Model 2-1	1732.51	$2.94 \times 10^{-11} \pm 1.5 \times 10^{-30}$

Figure Captions:

Fig. 1 (a) Schematic of the possible heterogeneous twinning sites; (b) schematic for force balances at the TJ's for model 1-2, model 2-1 and model 2-2.

Fig. 2 (a) The facet-facet/wall groove; (b) the top view of the nucleus and the force balances required at the TJ's; (c) the final shape of the truncated nucleus on facet 1 for model 1-1. In Fig. 2(c), the angles, normal to the facet, with the superscript prime indicate they are defined at the top surface of the nucleus.

Fig. 3 (a) Free energy of formation for a faceted nucleus with a facet angle $\nu_1 = 150°$ for an undercooling of 2.8 K in both models ; $\sigma_{GB} = 0.4842$ J/m^2 ; (b) free energy of formation for a twinned nucleus with a facet angle $\nu_1 = 150°$ for an undercooling of 2.8 K in both models ; $\sigma_{GB} = 0.4842$ J/m^2 and $\sigma_{twin} = 2$ mJ/m^2 ; (c) twinning probability at the facet angle $\nu_1 = 150°$ as a function of the undercooling at $\sigma_{GB} = 0.4842$ J/m^2 and $\sigma_{\text{twin}} = 2$ mJ/m^2.

Fig. 4 Effect of the facet angles on the twinning probability as a function of the undercooling for model 1-1 with $\sigma_{\text{twin}} = 2$ mJ/m^2.

Fig. 5 (a) EBSD IPF (Inverse Pole Figure) map along the growth direction of the grain structure after growth from a seed oriented <100> from the experiment described in details in [2, 19] ; (b) zoom in a region of twin nucleation corresponding Case 1 (grain boundary groove); (c) zoom in a region of twin nucleation corresponding Case 2 (edge {111} facet).

Fig. 6 (a) EBSD IPF (Inverse Pole Figure) map along the growth direction of the grain structure after growth from a seed oriented <110> from the experiment described in details in [1]. Twin grain growth from SLG TJ (Case 3); (b)

schematic showing the twin formation at the solid-liquid interface during directional solidification for Case 3.

Fig.1

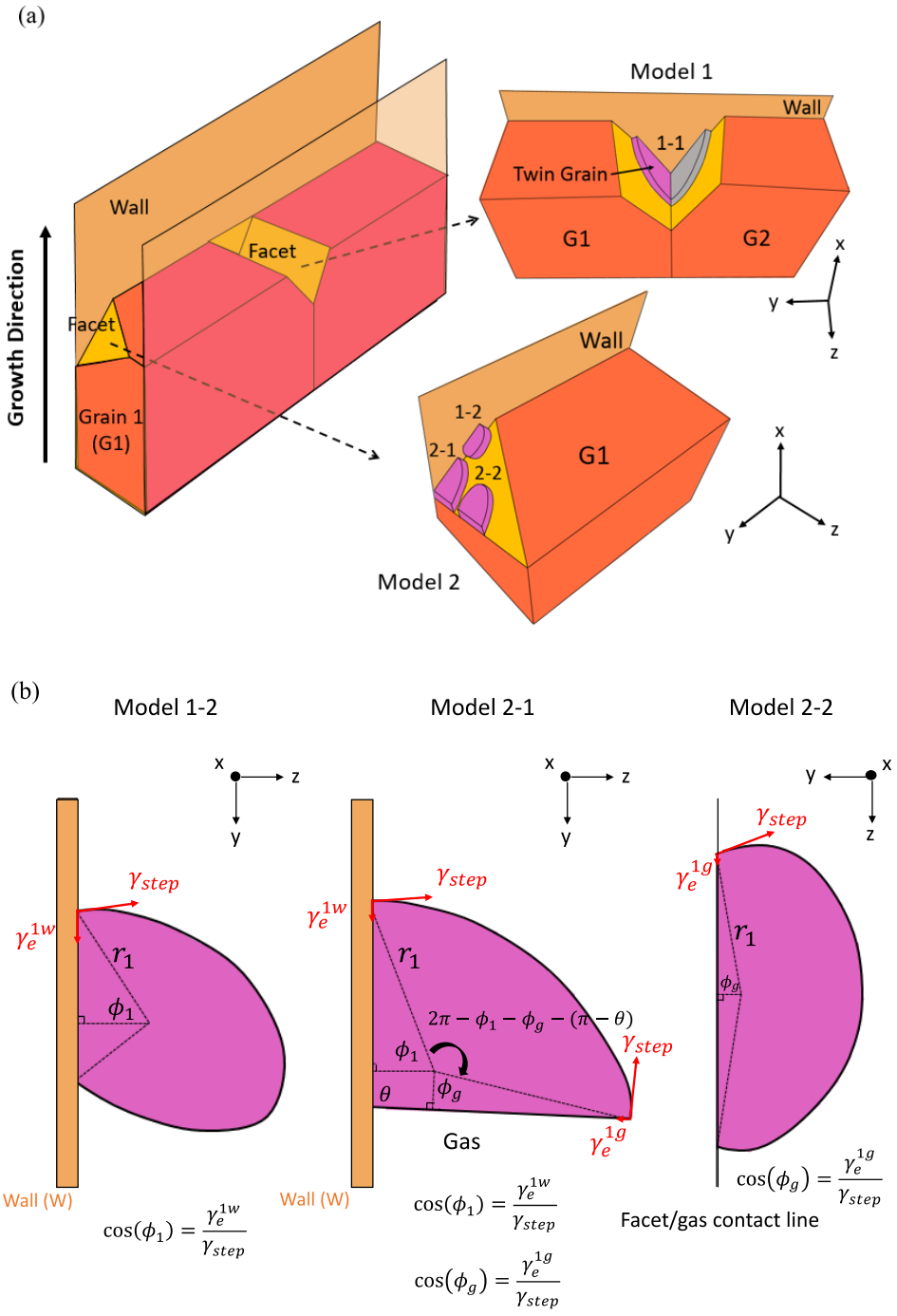

Fig. 1 (a) Schematic of the possible heterogeneous twinning sites; (b) schematic for force balances at the TJ's for model 1-2, model 2-1 and model 2-2.

Fig.2

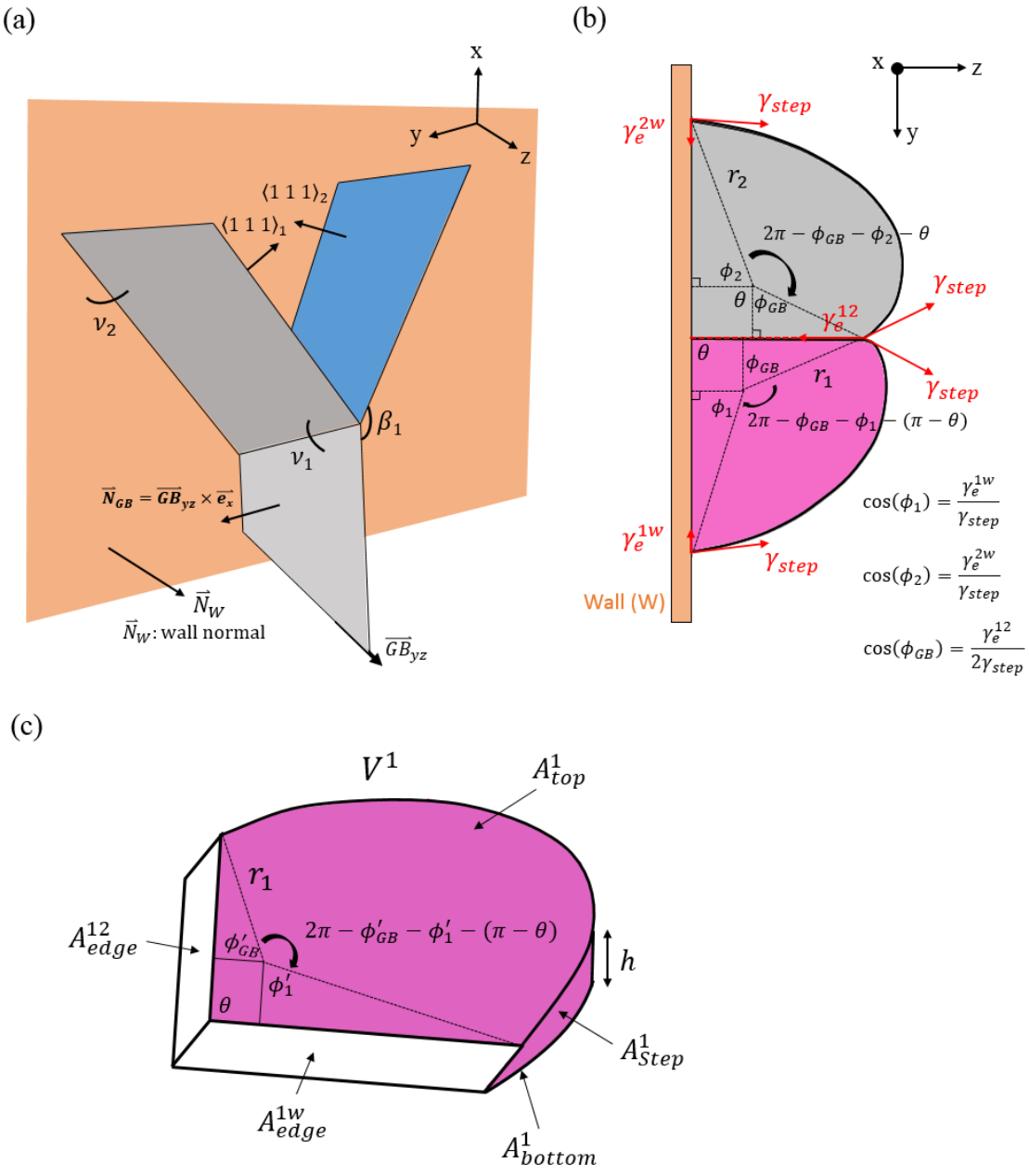

Fig. 2 (a) The facet-facet/wall groove; (b) the top view of the nucleus and the force balances required at the TJ's; (c) the final shape of the truncated nucleus on facet 1 for model 1-1. In Fig. 2(c), the angles, normal to the facet, with the superscript prime indicate they are defined at the top surface of the nucleus.

Fig.3

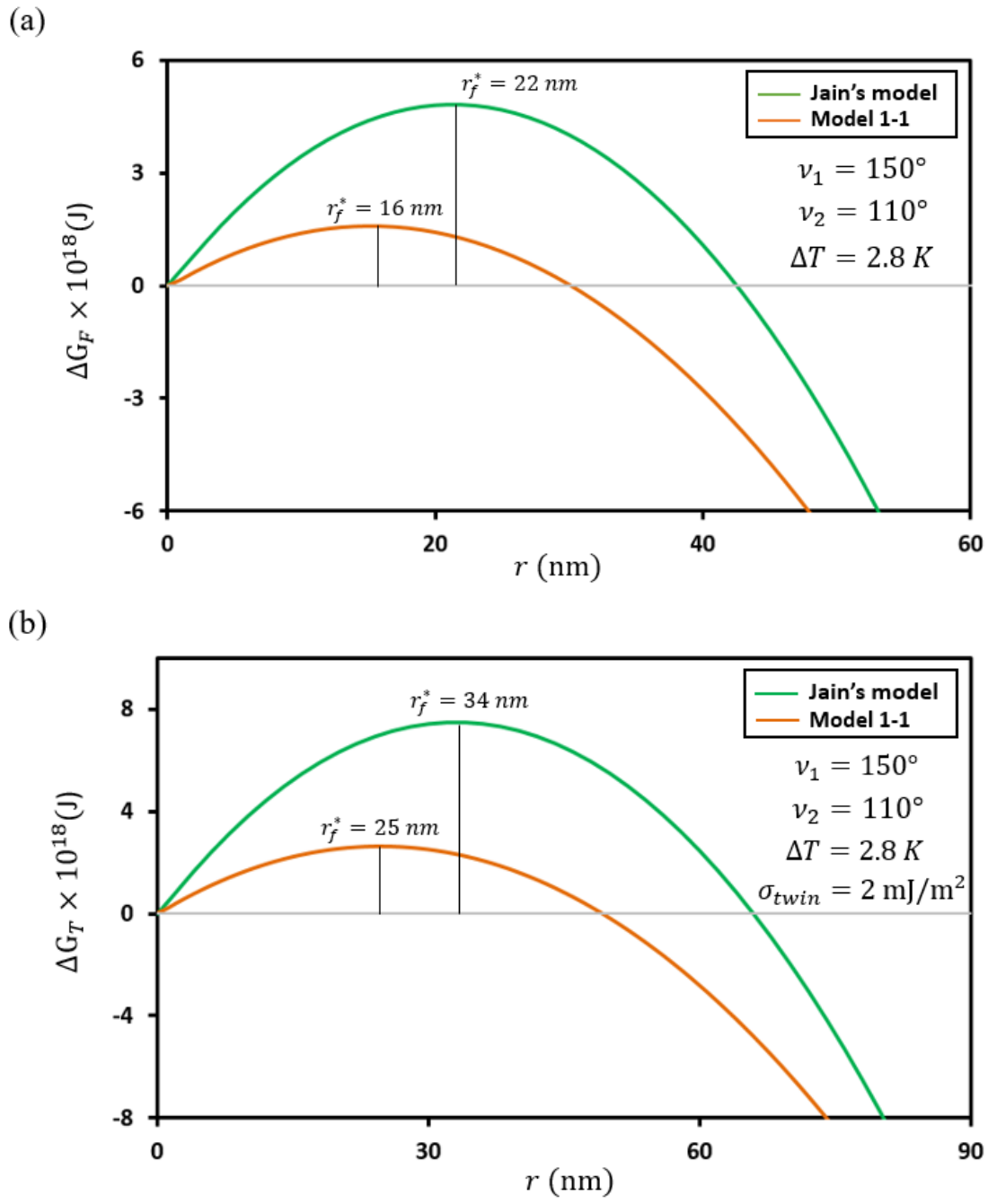
(a)
$r_f^* = 22\ nm$
$r_f^* = 16\ nm$
Jain's model
Model 1-1
$\nu_1 = 150°$
$\nu_2 = 110°$
$\Delta T = 2.8\ K$
$\Delta G_F \times 10^{18}$(J)
r (nm)
(b)
$r_f^* = 34\ nm$
$r_f^* = 25\ nm$
Jain's model
Model 1-1
$\nu_1 = 150°$
$\nu_2 = 110°$
$\Delta T = 2.8\ K$
$\sigma_{twin} = 2$ mJ/m^2
$\Delta G_T \times 10^{18}$(J)
r (nm)

(c)

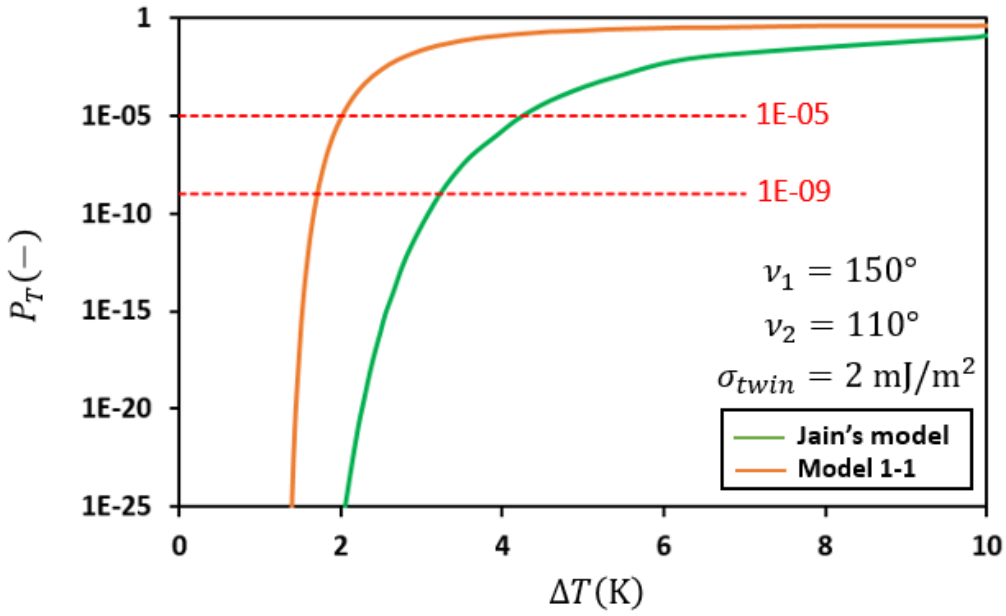

Fig. 3 (a) Free energy of formation for a faceted nucleus with a facet angle $\nu_1 = 150°$ for an undercooling of 2.8 K in both models；$\sigma_{GB} = 0.4842$ J/m^2；(b) free energy of formation for a twinned nucleus with a facet angle $\nu_1 = 150°$ for an undercooling of 2.8 K in both models；$\sigma_{GB} = 0.4842$ J/m^2 and $\sigma_{\mathrm{twin}} = 2$ mJ/m^2；(c) twinning probability at the facet angle $\nu_1 = 150°$ as a function of the undercooling at $\sigma_{GB} = 0.4842$ J/m^2 and $\sigma_{twin} = 2$ mJ/m^2.

Fig.4

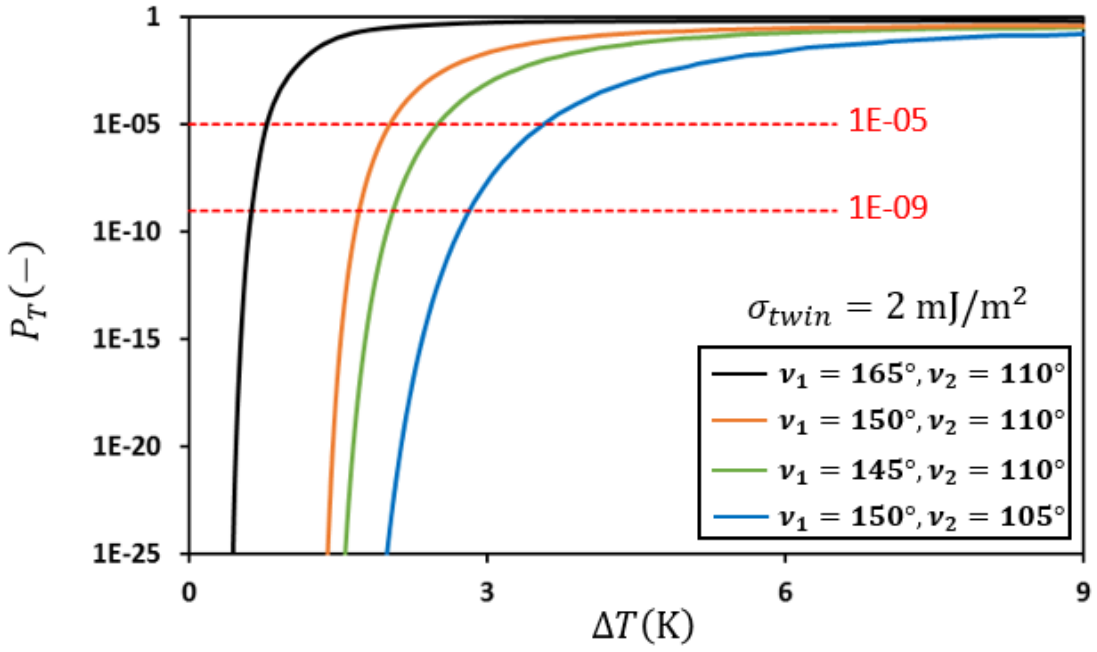

Fig. 4 Effect of the facet angles on the twinning probability as a function of the undercooling for model 1-1 with $\sigma_{\text{twin}} = 2$ mJ/m^2.

Fig.5

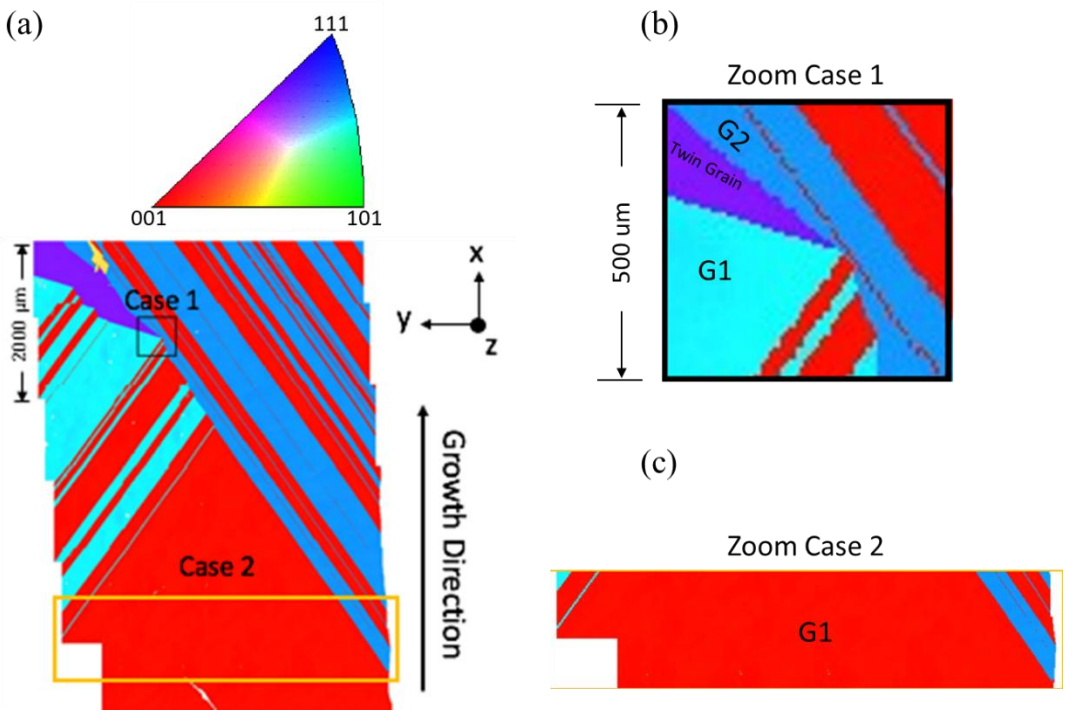

Fig. 5 (a) EBSD IPF (Inverse Pole Figure) map along the growth direction of the grain structure after growth from a seed oriented <100> from the experiment described in details in [2, 19]；(b) zoom in a region of twin nucleation corresponding Case 1 (grain boundary groove)；(c) zoom in a region of twin nucleation corresponding Case 2 (edge {111} facet).

Fig.6

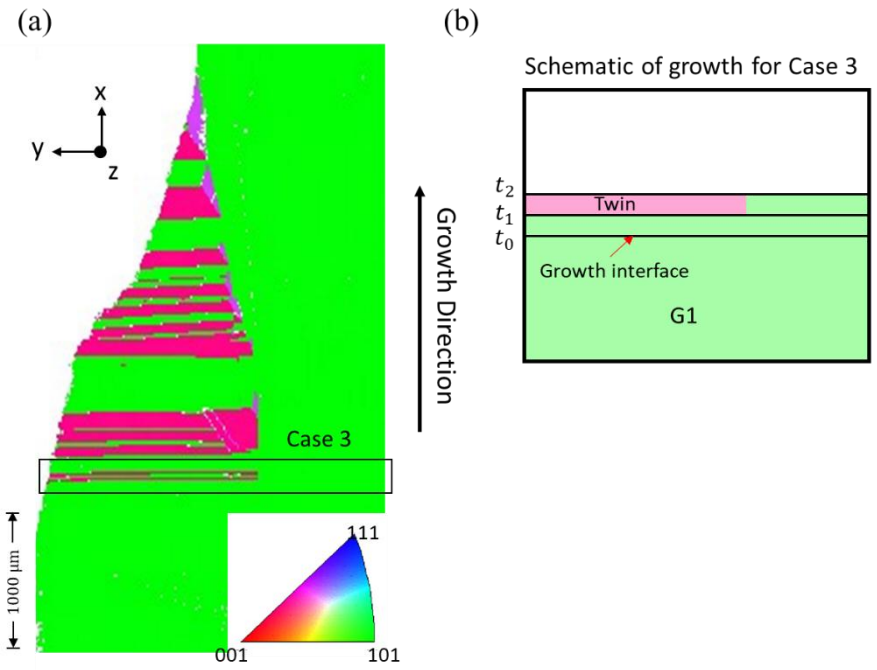

Fig. 6 (a) EBSD IPF (Inverse Pole Figure) map along the growth direction of the grain structure after growth from a seed oriented <110> from the experiment described in details in [1]. Twin grain growth from SLG TJ (Case 3)；(b) schematic showing the twin formation at the solid-liquid interface during directional solidification for Case 3.